

Detecting short-term gravitational waves from post-merger hyper-massive neutron stars with a kilohertz detector

Yikang Chen(陈奕康) and Zong-Hong Zhu(朱宗宏)

Citation: Chin. Phys. B, 2024, 33 (**8**): 080401. DOI: 10.1088/1674-1056/ad5320
Journal homepage: http://cpb.iphy.ac.cn; http://iopscience.iop.org/cpb

What follows is a list of articles you may be interested in

Optimal zero-crossing group selection method of the absolute gravimeter based on improved auto-regressive moving average model

Zonglei Mou(牟宗磊), Xiao Han(韩笑), and Ruo Hu(胡若)
Chin. Phys. B, 2023, 32 (**11**): 110401. DOI: 10.1088/1674-1056/ace4b5

Silicon photomultiplier based scintillator thermal neutron detector for China Spallation Neutron Source (CSNS)

Xiu-Ping Yue(岳秀萍), Zhi-Fu Zhu(朱志甫), Bin Tang(唐彬), Chang Huang(黄畅), Qian Yu(于潜), Shao-Jia Chen(陈少佳), Xiu-Ku Wang(王修库), Hong Xu(许虹), Shi-Hui Zhou(周诗慧),Xiao-Jie Cai(蔡小杰), Hao Yang(杨浩), Zhi-Yong Wan(万志勇),Zhi-Jia Sun(孙志嘉), and Yun-Tao Liu(刘云涛)
Chin. Phys. B, 2023, 32 (**9**): 090402. DOI: 10.1088/1674-1056/ace316

Application of Newtonian approximate model to LIGO gravitational wave data processing

Jie Wu(吴洁), Jin Li(李瑾), and Qing-Quan Jiang(蒋青权)
Chin. Phys. B, 2023, 32 (**9**): 090401. DOI: 10.1088/1674-1056/acd8a3

Simulation of the gravitational wave frequency distribution of neutron star-black hole mergers

Jianwei Zhang(张见微), Chengmin Zhang(张承民), Di Li(李荻), Xianghan Cui(崔翔翰), Wuming Yang(杨伍明), Dehua Wang(王德华), Yiyan Yang(杨佚沿), Shaolan Bi(毕少兰), and Xianfei Zhang(张先飞)
Chin. Phys. B, 2021, 30 (**12**): 120401. DOI: 10.1088/1674-1056/abff28

High-frequency gravitational waves having large spectral densities and their electromagnetic response

Li Fang-Yu (李芳昱), Wen Hao (文毫), Fang Zhen-Yun (方祯云)
Chin. Phys. B, 2013, 22 (**12**): 120402. DOI: 10.1088/1674-1056/22/12/120402

Detecting short-term gravitational waves from post-merger hyper-massive neutron stars with a kilohertz detector

Yikang Chen(陈奕康)[1,2] and Zong-Hong Zhu(朱宗宏)[1,2,†]

[1] *Institute for Frontier in Astronomy and Astrophysics, Beijing Normal University, Beijing* 102206, *China*
[2] *Department of Astronomy, Beijing Normal University, Beijing* 100875, *China*

(Received 14 March 2024; revised manuscript received 12 May 2024; accepted manuscript online 3 June 2024)

Gravitational waves emanating from binary neutron star inspirals, alongside electromagnetic transients resulting from the aftermath of the GW170817 merger, have been successfully detected. However, the intricate post-merger dynamics that bridge these two sets of observables remain enigmatic. This includes if, and when, the post-merger remnant star collapses to a black hole, and what are the necessary conditions to power a short gamma-ray burst, and other observed electromagnetic counterparts. Our focus is on the detection of gravitational wave (GW) emissions from hyper-massive neutron stars (NSs) formed through binary neutron star (BNS) mergers. Utilizing several kilohertz GW detectors, we simulate BNS mergers within the detection limits of LIGO-Virgo-KARGA O4. Our objective is to ascertain the fraction of simulated sources that may emit detectable post-merger GW signals. For kilohertz detectors equipped with a new cavity design, we estimate that approximately 1.1%–32% of sources would emit a detectable post-merger GW signal. This fraction is contingent on the mass converted into gravitational wave energy, ranging from $0.01M_{\rm sun}$ to $0.1M_{\rm sun}$. Furthermore, by evaluating other well-regarded proposed kilohertz GW detectors, we anticipate that the fraction can increase to as much as 2.1%–61% under optimal performance conditions.

Keywords: neutron star mergers, gravitational waves

PACS: 04.30.–w, 04.80.Nn, 97.60.Jd **DOI:** 10.1088/1674-1056/ad5320

1. Introduction

On 17 August 2017, the LIGO and Virgo detectors detected a gravitational wave signal, GW170817, emanating from a binary neutron star system. This unprecedented observational campaign motivated a series of investigations into the implications for astrophysics, dense nuclear matter, gravity, and cosmology,[1] such as the resonant scattering of gravitational waves with electromagnetic waves,[2] the estimation of far-field wavefront error of tilt-to-length distortion coupling in space-based gravitational wave detection,[3] and applications of the Newtonian approximate model to LIGO gravitational wave data processing.[4] Around 1.7 s after the merger, Fermi's Gamma-ray Burst Monitor detected a gamma-ray burst, GRB170817A,[5] and began electromagnetic follow-up observations.[6]

The gravitational wave (GW) emission following the merger of a binary neutron star (BNS) system depends on the type of central remnant. According to theory, there are four potential evolutionary paths for the central remnant:[7–16] (1) immediate collapse into a black hole (BH); (2) formation of a differentially rotating hyper-massive neutron star (HMNS), which collapses into a BH within seconds; (3) formation of a differentially rotating HMNS that transitions into a rigidly rotating super-massive neutron star (SMNS) after the differential rotation disappears (it then collapses into a BH once the SMNS spins down); (4) formation of a stable neutron star (SNS) following the HMNS phase.

During BNS-merger simulations, if an HMNS is formed, it is anticipated to emit a significant amount of post-merger GWs, primarily influenced by the quadrupolar f-mode. This emission typically has a frequency range spanning approximately 2 kHz to 4 kHz.[17–20] In reality, depending on the equation of state of neutron stars, the post-merger GW emission can commence at around 1 kHz.[21] However, this GW emission rapidly diminishes within approximately 100 ms due to either the collapse of the HMNS into a BH (route 2) or the formation of a rigidly rotating neutron star (NS) (routes 3 and 4).[9,20,22–24] In some cases, the BNS birthrate and merge rate, as well as the mass range of merged BNS, also need to be considered.[25] To detect the post-merger signal of binary neutron stars, it is necessary to employ the upgraded GW detectors to scour for the enduring post-merger signals, particularly those detectors that possess peak sensitivity within the kilohertz range.

By treating the arm cavity and the signal recycling cavity as a coupled system, it has been demonstrated that lengthening the signal recycling cavity can effectively shift the sensitive frequency band towards higher frequencies.[26] Furthermore, by directly adjusting the phase of the signal recycling mirror, we can dynamically control the resonance frequency of the GW detector. However, this approach may result in a reduced response to incoming signals, as one of the sidebands may not be captured by the photo detector.[27]

[†]Corresponding author. E-mail: zhuzh@bnu.edu.cn

© 2024 Chinese Physical Society and IOP Publishing Ltd

This paper introduces an improved design based on Advanced LIGO, which emerged after a thorough examination and comparison of previous strategies. An auxiliary triangular resonance cavity, serving as an "attachment", has been installed on the interferometer. Its primary function is to compensate for the phase shift achieved by lengthening the signal recycling cavity (SRC). The significant advantage of this attachment is that it allows Advanced LIGO to maintain its original design without it. When the attachment is integrated into the detector, it produces the same effect as extending the length of the signal recycling cavity. However, it also introduces some new losses, leading to a slightly reduced sensitivity.

The paper is organized as follows: In Section 2, we describe the gravitational wave signal of the binary neutron-star post-merger. In Section 3, we investigate the distribution of red-shift related to BNS mergers. In Section 4, we present several designs to enhance the sensitivity of GW detectors in kilohertz. In Section 5, we deliberate on the viability of detecting this particular type of GWs using kilohertz GW detectors. Specifically, our objective is to determine the fraction of BNS mergers, identified by the present GW detector LIGO A^+, that would yield a detectable post-merger GW signal when different kilohertz detectors are employed. Finally, we conclude our findings and provide discussions in Section 6.

2. Signal of binary neutron-star postmerger

We simulate the postmerger waveform using a damped sinusoidal time domain waveform. The Fourier transform of this damped sinusoidal function is a Lorentzian function. This Lorentzian function has a symmetric composition of positive and negative frequency complex Lorentzian damped envelopes:

$$\tilde{h}_{\rm DS}(f) = \sqrt{\frac{H}{4\pi}}\cdot\frac{{\rm e}^{{\rm i}\theta(f)}\sqrt{f_0/Q}}{f_0/2Q+{\rm i}(f-f_0)} + \sqrt{\frac{H}{4\pi}}\cdot\frac{{\rm e}^{-{\rm i}\theta(f)}\sqrt{f_0/Q}}{f_0/2Q-{\rm i}(f-f_0)}. \tag{1}$$

The total energy of the strain signal is represented by H; and ${\rm e}^{{\rm i}\theta(f)}$ represents additional parameters in the phase response, which do not impact the calculation of the signal-to-noise ratio (SNR). The central frequency of the signal is denoted as f_0, and its bandwidth is determined by its quality factor Q.

$$E_{\rm GW} = \frac{c^3}{G}\frac{4}{5}\pi^2 D^2 f_0^2 H. \tag{2}$$

There is a correlation between the strain signal energy H and the energy converted into gravitational wave energy postmerger, denoted as $E_{\rm PM}$.

$$H = (2\pi f_0 D)^{-2}\frac{5G}{c^3}E_{\rm PM}, \tag{3}$$

where D is the distance to the source, G is gravitational constant, and c is the speed of light in vacuum. $E_{\rm PM}$ can be described by the mass $M_{\rm PM}$ that is converted into gravitational wave energy during the postmerger. We assume that the binary neutron star system is located at a distance of 50 Mpc and $M_{\rm PM} = 0.1M_{\rm sun}$. Based on these assumptions, the value of H can be estimated by

$$H \approx 7.27\times10^{-46}\Big(\frac{1.8\ {\rm kHz}}{f_0}\Big)^2\Big(\frac{50\ {\rm MPC}}{\rm D}\Big)^2\frac{M_{\rm PM}}{0.1M_{\rm sun}}, \tag{4}$$

where f_0 and Q can be simulated by using the equation of state, total mass, and the mass ratio of the binary neutron star system. The final binary neutron-star postmerger signal can be synthesized using the above-mentioned calculated parameters H, Q, and f_0. By using this signal, we can adjust the appropriate detector parameters to calculate the signal-to-noise ratio (SNR). The SNR of the detector is calculated as follows:

$${\rm SNR} = 2\sqrt{\int_{-\infty}^{\infty}{\rm d}f\frac{|\tilde{h}_{\rm DS}(f)|^2}{S_{\rm hh}(f)}}, \tag{5}$$

where $S_{\rm hh}(f)$ is the power spectral density of the detector. It is determined by the configuration of GW detector.

3. distribution of redshift

The red-shift distribution of BNS mergers is determined by the BNS merger rate at each red shift. Typically, the BNS merger rate in a given volume follows the star formation rate (SFR), with a time delay between the formation of the BNS system and its merger.[28,29] This relationship can be written as

$$R_{\rm merger}(z) = R_{\rm merger,0}\int_0^z f(z')G(\tau)\frac{{\rm d}\tau}{{\rm d}z}{\rm d}z', \tag{6}$$

where $f(z) = {\rm SFR}(z)/{\rm SFR}(z=0)$ is the normalized SFR, with the SFR fitted as[30]

$${\rm SFR}(z) \propto g(z,\eta)^{1/\eta}, \tag{7}$$

$$g(z,\eta) = (1+z)^{3.4\eta} + \Big(\frac{1+z}{3000}\Big)^{-0.3\eta} + \Big(\frac{1+z}{9}\Big)^{-3.5\eta}. \tag{8}$$

When $\eta = -10$ is chosen, τ represents the time delay, and $G(\tau)$ defines its probability density function. Suppose that the time delay follows a log-normal distribution, as reported in Refs. [28,29].

$$G(\tau) = \frac{1}{\sqrt{2\pi}\sigma_\tau\tau}\exp\Big(\frac{\ln\tau-\ln\tau_{\rm d}}{2\sigma_{\rm tau}^2}\Big), \tag{9}$$

where $\tau_{\rm d} = 2.9$ Gyr and $\sigma_\tau = 0.2$ ln(Gyr). The BNS merger rate in a specific radial shift bin can be determined by

$${\rm d}\dot{N}(z) = \frac{R_{\rm merger}(z)}{1+z}\frac{{\rm d}V}{{\rm d}z}{\rm d}z, \tag{10}$$

where V is the comoving volume of the universe and

$$\frac{\mathrm{d}V(z)}{\mathrm{d}z} = 4\pi\left(\frac{c}{H_0}\right)^3\left(\int_0^z \frac{\mathrm{d}z}{\sqrt{1-\Omega_\mathrm{m}+\Omega_\mathrm{m}(1+z)^3}}\right)^2 \times \frac{1}{\sqrt{1-\Omega_\mathrm{m}+\Omega_\mathrm{m}(1+z)^3}}. \tag{11}$$

with $H_0 = 68.7\ \mathrm{km{\cdot}s^{-1}{\cdot}Mpc^{-1}}$ and $\Omega_\mathrm{m} = 0.308$ adopted.[31]

4. Configuration of high-frequency gravitational wave detector

4.1. Long SRC interferometer

By adjusting the resonance frequency of the detector to match the signal's high frequency, it is possible to achieve better sensitivity. The signal recycling cavity (SRC) and arm cavity can be considered as a coupled cavity for calculating phase shift. Therefore, the first strategy is to extend the length of the SRC.[26] The phase shift of the arm cavity to the signal remains constant based on the configuration of Advanced LIGO. This means that the resonant frequency of the detector can be controlled by modifying the length of the SRC.

We aim to adjust the resonance frequency of the Arm-SRC coupled cavity to approximately 1.9 kHz.[27] This resonance frequency enhances the interferometer's response to gravitational waves generated by the postmerge of binary neutron stars. The phase shift of light, which is achieved by reflecting it off the arm cavity, can be calculated by

$$\phi_\mathrm{arm}(\Omega) = \mathrm{atan}\frac{\Omega}{\gamma_\mathrm{arm}}, \tag{12}$$

$$\gamma_\mathrm{arm} = \frac{cT_\mathrm{arm}}{4L_\mathrm{arm}}, \tag{13}$$

where $\Omega = 2\pi f$ is the sideband frequency, and γ_arm is the arm cavity bandwidth.

The phase shift of light reflected from the arm cavity and the phase shift of light passing through the SRC must be summed to achieve resonance conditions. It can be calculated as follows:

$$\phi_\mathrm{arm}(\Omega) + \phi_\mathrm{src}(\Omega) = \pi, \tag{14}$$

$$\phi_\mathrm{src}(\Omega) = \frac{2\Omega L_\mathrm{src}}{c}, \tag{15}$$

where L_src represents the length of SRC, it can be calculated to be 550 m based on this template of configuration. The main parameters of this template are presented in the form of Table 1. Additionally, we provide the sensitivity curve of this template in Fig. 1.

4.2. Tuning advanced LIGO to kilohertz signals

Instead of increasing the length of SRC, we can also directly introduce the required phase shift by tuning the phase of SRC. In this case, Eq. (14) is modified to

$$\phi_\mathrm{arm}(\Omega) + \phi_\mathrm{src}(\Omega) + \phi_\mathrm{d} = \pi. \tag{16}$$

In this configuration, ϕ_d is the tuning phase, which makes it convenient for the detector to adjust. By locking the SRC at different frequencies in experiments, the resonance frequency of the detector to the signal can be flexibly shifted. In this way, the resonance frequency of the SRC can be shifted to the desired high frequency. The greatest advantage of this configuration lies in its ease of adjustment and flexibility in shifting the resonance frequency, which is crucial for practical applications.

When the detuning is optimized for resonance in the high-frequency region, an additional narrow-band optomechanical spring resonance is formed at low frequencies. However, in general, this effect has minimal impact on detecting the post-merger signal from binary neutron stars. The detuned configuration exhibits different effects for different sources,[27] demonstrating that this configuration is most effective for MQLF-type signals.

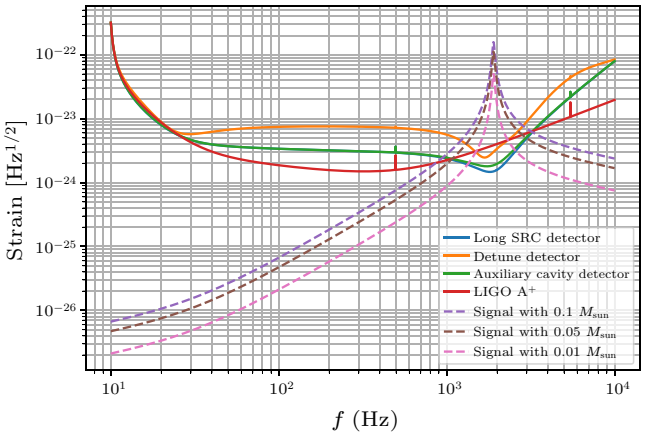


Fig. 1. Sensitivity curves for the designed kilohertz GW detectors (solid lines) and the strain for h_DS (dashed lines) in the frequency domain. For comparison, the sensitivity curve for LIGO A$^+$ is also shown. We adopt the parameters for the post-merger NS as $f_0 = 1900$ Hz and $Q = 30$, observed at 50 Mpc. For the masses converted to gravitational wave energy during postmerger, $M_\mathrm{pm} = 0.01\ M_\mathrm{sun}$, $0.05M_\mathrm{sun}$, and $0.1M_\mathrm{sun}$ are assumed. It is plotted in spectral density units using the form of $2\sqrt{f}|\tilde{h}_\mathrm{DS}(f)|$.

Furthermore, the filter cavity is essential for the detuned configuration when the squeezing part is utilized. Unlike other configurations, the squeezing angle necessitates adjustment to accommodate the tuning phase. The parameters for this template are listed in Table 1. Additionally, we present the sensitivity curve of this template in Fig. 1.

4.3. Using a new auxiliary cavity

The length of SRC in the Advanced LIGO detector is 55 m. The optimal detection frequency band for the Advanced LIGO detector ranges from 10 Hz to 300 Hz. Based on the above description, increasing the length of SRC can shift the optimal detection frequency band towards higher frequencies.

However, in practical experimental operations, adjusting the length of SRC is not a straightforward task. Additionally,

high-frequency gravitational wave detectors often exhibit limitations in low-frequency detection. Therefore, when the detection range needs to be modified, an auxiliary resonance cavity can be integrated into the main interferometer without altering the parameters of the Advanced LIGO detector. As illustrated in Fig. 2.

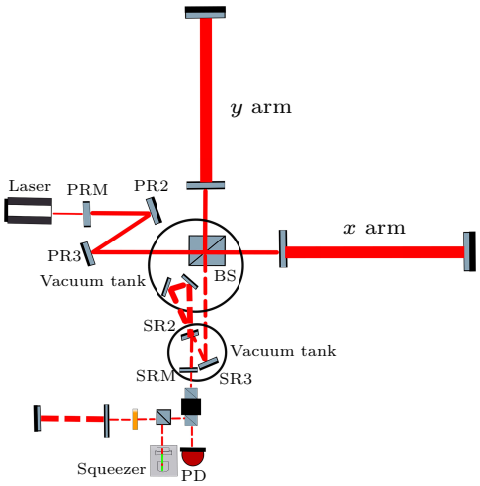


Fig. 2. Schematic of dual-recycled Michelson interferometer. An auxiliary cavity is attached to one folding mirror within signal recycling cavity.

This configuration of detector also needs to satisfy resonance conditions. In this case, Eq. (14) is modified as

$$\phi_{\rm arm}(\Omega)+\phi_{\rm src}(\Omega)+\phi_x=\pi, \tag{17}$$

$$\phi_x(\Omega)=\operatorname{atan}\frac{\Omega}{\gamma_x}, \tag{18}$$

$$\gamma_x=\frac{cT_x}{4L_x}, \tag{19}$$

where ϕ_x is the phase shift provided by the auxiliary cavity, γ_x is the cavity bandwidth, and T_x and L_x are the transmission of SR2 and length of the auxiliary cavity in Fig. 2. Equation (19) reveals a relationship between T_x and L_x. When it comes to design, we aim to minimize the size of this auxiliary cavity. However, if L_x is too short, T_x will also be minimal, leading to the losses (Λ_x) in the auxiliary cavity and a decrease in detector sensitivity. To achieve a balance, we have chosen the following parameters for the auxiliary cavity: $L_x=15$ m and $T_x=0.12$. When utilizing this configuration to actively incorporate a triangular resonance cavity, it is crucial to account for some additional losses. The extra loss incurred in the new cavity, denoted as $\Lambda_{\rm new}$, can be computed as follows:

$$\Lambda_{\rm new}=5\ {\rm m}\times 3\ {\rm ppm/m}\times 3\times\frac{4}{T_x}=0.15\%. \tag{20}$$

Therefore, the total loss of SRC is the sum of this additional loss and the original SRC loss. We simply classify the parameters of the detector into three categories: main interferometer or arm cavity part, signal recycling cavity part and squeezing part. The parameters of the arm cavity mainly affect the circulating power and finesse, which determine the overall sensitivity of the detector. We used the parameters of Advanced LIGO without changing them. For the signal recycling cavity part, we calculated the parameters according to the method previously mentioned to obtain the kHz detector, which is essentially to sacrifice the sensitivity at low frequency to obtain the sensitivity at high frequency. The parameters of the squeezer and filter cavity also need to be adjusted based on the values of the previous two parts. The parameters for this template are listed in Table 1. Furthermore, we present the sensitivity curve of this template in Fig. 1.

Table 1. Parameters of three types of detector.

Parameters	Long SRC	Detuned	New cavity
Arm length, $L_{\rm arm}$	4 km	4 km	4 km
Arm transmission, $T_{\rm arm}$	0.014	0.014	0.014
SRC length, $L_{\rm src}$	550 m	55 m	55+15 m
SRC transmission, $T_{\rm src}$	0.03	0.03	0.03
SRC loss, $\Lambda_{\rm SRC}$	0.1%	0.1%	0.1+0.15%
SRC detuning, $\phi_{\rm src}$	0°	2.4°	0°
Injected squeezing	12 dB	12 dB	12 dB
Injection loss	5%	5%	5%
Readout loss	10%	10%	10%
Filter cavity length	300 m	1000 m	300 m
Filter cavity loss	60 ppm	15 ppm	60 ppm
Filter cavity transmission	0.0003	0.0535	0.0003
Filter cavity detuning	13 Hz	1759 Hz	13 Hz

5. Detectability

In this study, we concentrate our attention on the BNS mergers that are detectable during LIGO-Virgo-KAGRA O4, which has a detection limit of 170 Mpc.[32] Our aim is to determine the proportion of these identified BNS mergers that may be accompanied by a detectable post-merger GW emission.

We randomly generate a total of 50000 BNS merger systems within a distance of 170 Mpc, adhering strictly to the red-shift distribution described in Section 3. Technically speaking, all our simulated sources reside in the nearby universe, where the event rate density, denoted as $R_{\rm merger}$, remains constant across various redshifts. Although the aforementioned approach for computing the red-shift distribution may be overkill, we utilize it for its generality. For the GW sources, we adopt the MQLF-type signals, as cited in Ref. [27]. The parameters are as follows: $f_0=1900$ Hz and $Q=30$.

Since there is no definitive conclusion regarding the mass converted into gravitational wave energy during post-merger ($E_{\rm PM}$), we utilize observational data from GW170817[1] to estimate the masses as $M_{\rm pm}=0.01M_{\rm sun}$, $0.05M_{\rm sun}$, and $0.1M_{\rm sun}$. Subsequently, we proceed to calculate the characteristic strain of the GW radiation and its signal-to-noise ratio (SNR) using a specific GW detector. By establishing a threshold SNR for each detector, we determine the number of sources with a de-

tectable post-merger GW signal and record the corresponding fraction.

The cumulative distribution of signal-to-noise ratios (SNRs) for post-merger gravitational waves is presented in the left panels of Fig. 3 for various kilohertz GW detectors. Additionally, the distribution of SNR is demonstrated when employing LIGO A$^+$ to detect post-merger GWs. By setting a threshold of SNR > 8, the proportion of simulated sources exhibiting a detectable post-merger GW signal can be determined. These percentages are tabulated in Table 2.

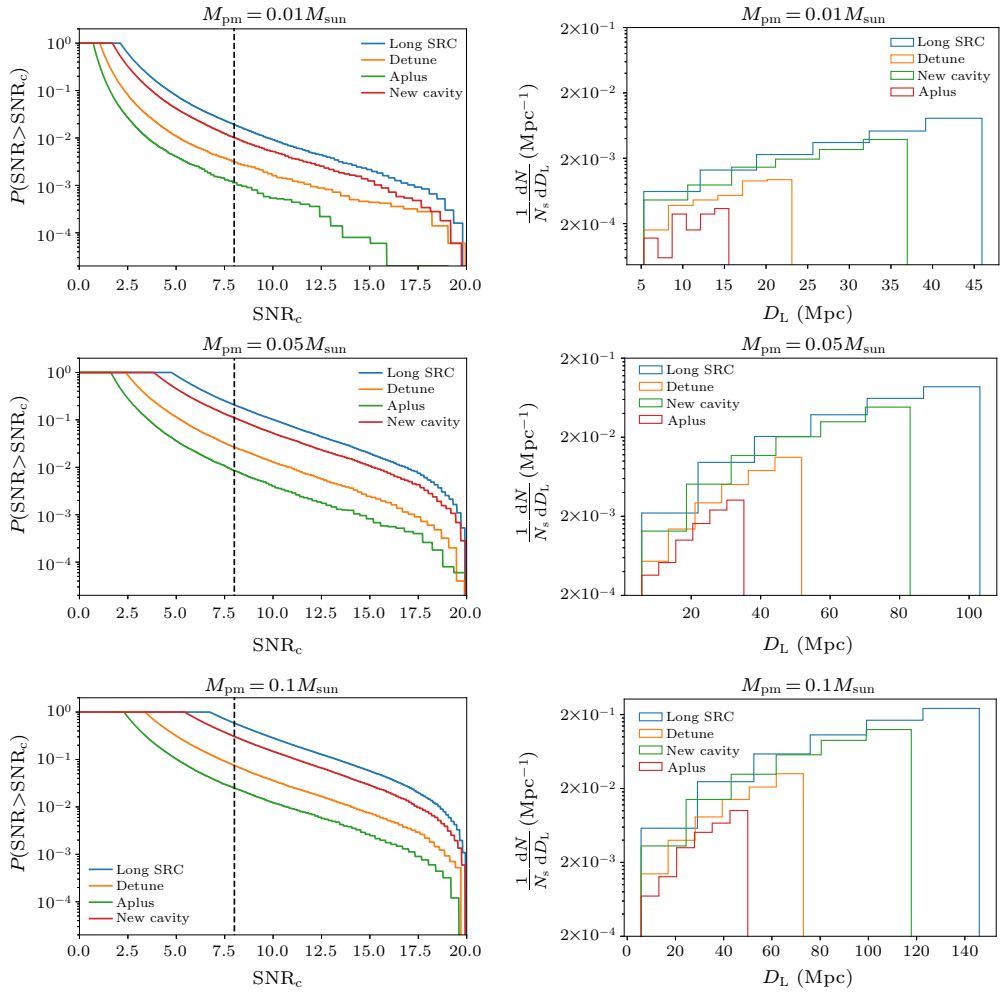


Fig. 3. The left panels show the cumulative SNR distribution for the simulated post-merger GW signals, and the right panels show the distribution of the distances from the GW sources to the observer for those with SNR > 8. The upper, middle and lower panels show the cases of $M_{\rm pm} = 0.01M_{\rm sun}$, $0.05M_{\rm sun}$, and $0.1M_{\rm sun}$, respectively. Different colors stand for different GW detectors applied.

Table 2. The fraction of BNS mergers, inside the detecting limit of LIGO-Virgo-KAGRA O4 (170 Mpc), with a detectable post-merger GW signal.

$M_{\rm pm}$	$0.01M_{\rm sun}$	$0.05M_{\rm sun}$	$0.1M_{\rm sun}$
LIGO A$^+$	0.12%	0.91%	2.7%
Long SRC	2.1%	22%	61%
Detune	0.34%	2.9%	8.0%
New cavity	1.1%	12%	32%

The results indicate that, as the mass converted into gravitational wave energy during the post-merger phase ($M_{\rm PM}$) increases, the fraction of sources exhibiting detectable post-merger GW signals also rises for all detectors. This finding is rationalized by the fact that the strain of the gravitational wave signal energy, denoted as $h_{\rm DS}$, becomes more significant, leading to enhanced integral signal-to-noise ratios (SNRs). The histogram depicting the distances of all sources exhibiting a detectable post-merger GW signal is presented in the right panels of Fig. 3. The vertical axes have been normalized based on the total number of simulated sources. As evident from the figure, for secular post-merger GW signals, the detection rate may not always scale proportionally with the cube of a detector's detection limit. This is because the detection limit is primarily determined by GWs emitted from SNSs, whereas some high-frequency detectors may also exhibit sensitivity towards sources collapsing at earlier stages.

The performance of the kilohertz GW detectors is satisfactory when compared to LIGO Aplus. Specifically, when the post-merger mass ($M_{\rm pm}$) is set to $0.1M_{\rm sun}$, a significant fraction ranging from 8% to 61% of the BNS sources identified

during the LIGO-Virgo-KAGRA O4 observation period can potentially emit a detectable post-merger GW signal. Even under the assumption of a much lighter post-merger mass of $0.01M_{\rm sun}$, the new cavity kilohertz GW detector can still detect more than 1% of these sources. Among all the detectors considered, the long-SRC detector exhibits the most promising performance solely based on its detection rate.

6. Discussion and conclusion

In summary, we have conducted a detailed study on the gravitational wave emissions that arise from the newly formed neutron stars resulting from binary neutron star mergers. We delve into the discussion of several kilohertz GW detectors specifically designed to target this type of signal. Furthermore, we simulate BNS mergers within the detection limit of the LIGO-Virgo-KAGRA O4 network (170 Mpc) and infer the proportion of sources that exhibit a detectable long-term post-merger GW signal for each individual kilohertz GW detector. This analysis aims to assess the performance of these detectors. For GW signals, it is similar to GW170817. The difference is that LIGO-Virgo uses the method of matched filtering while we calculate it through formulas. We choose the MQLF signal model which is the best-suited signal model for the detuning detector. It is convenient for us to compare the detector performance of different design ideas.

For the proposed kilohertz GW detector utilizing a novel cavity, the maximum fraction of sources exhibiting a detectable post-merger GW signal is approximately $\sim 32\%$ when the post-merger mass $M_{\rm pm} = 0.1M_{\rm sun}$. As the mass converts into gravitational wave signals diminishes, this fraction reduces to a range of 1.1%–12%. These outcomes surpass those of another detuned GW detector and significantly outperform the approach of solely searching for post-merger GW signals within the data of LIGO Aplus. This improvement is rationalized by the fact that, in theory, the power spectrum density of the detuned GW detector at its peak frequency would be twice as high as the detector proposed in this paper due to the loss of half of the sideband.

The percentages tabulated in Table 2 reveal that the long SRC kilohertz GW detector demonstrates the best performance. Notably, the implementation of a new auxiliary resonant cavity allows for outstanding results without altering the interferometer's core structure. This design's key advantage lies in its ability to precisely adjust the resonant cavity's transmission, effectively limiting its scale within a defined space. This is achieved through the cavity's compensation for phase shifts, enabling us to attain the desired peak frequency. While the introduction of the auxiliary resonant cavity inevitably leads to additional losses and noises, resulting in a reduction of sensitivity, the ease it brings to experimental operations remains within an acceptable range. It can temporarily turn the initial interferometer into a kHz detector by adding a small resonance cavity, and it can also restore the original sensitivity of the detector by removing the small resonance cavity.

Furthermore, the parameters of the arm cavity mainly affect the circulating power and finesse, which determine the overall sensitivity of the detector. For example, as the circulating power increases, the Advanced LIGO can detect more BNS mergers. However, in pursuing this approach, it is crucial to consider the antenna response, which can potentially impact the SNR of the GW detector. Additionally, it is fascinating to explore the ultimate light intensity that the interferometer can endure. In this work, we only consider the GW signals of MQLF-type. If we consider all signals in the frequency domain, the values of f_0 and Q should be a distribution, but so far there is no clear conclusion about this distribution.

The sensitivity of the kilohertz GW detector proposed in this paper is limited to a narrow frequency band, and its scientific goal is to target specific high-frequency GW signals. Different central frequencies correspond to different detector parameters. If considering to detect a wide range of frequencies, a broadband detector such as the third-generation gravitational wave detector would be more suitable (Cosmic Explorer and Einstein Telescope). In future research, the constraints on EOS will help us simulate the GW signals more accurately and we can estimate the tidal deformability measurement accuracy because the GW peak frequency is strongly correlated with the tidal deformability and star's compactness.

Acknowledgments

We are grateful to Teng Zhang, Shunke Ai, and Bin Liu for the idea and constructive discussion. This project was supported by the National Natural Science Foundation of China (Grant Nos. 12021003, 11920101003, and 11633001), and the Strategic Priority Research Program of the Chinese Academy of Sciences (Grant No. XDB23000000).

References

[1] Abbott B P *et al.* (LIGO Scientific Collaboration and Virgo Collaboration) 2017 *Phys. Rev. Lett.* **119** 161101
[2] Yan R D and Lau Y K 2023 *Chin. Phys. Lett.* **40** 100401
[3] Tao Y Z, Jin H B and Wu Y L 2023 *Chin. Phys. B* **32** 024212
[4] Wu J, Li J and Jiang Q Q 2023 *Chin. Phys. B* **32** 090401
[5] Abbott B P, Abbott R, Abbott T D, *et al.* 2017 *Astrophys. J. Lett.* **848** L13
[6] Abbott B P, Abbott R, Abbott T D, *et al.* 2017 *Astrophys. J. Lett.* **848** L12
[7] Rosswog S, Davies M B, Thielemann F K and Piran T 2000 *Astron. Astrophys.* **360** 171
[8] Rezzolla L, Baiotti L, Giacomazzo B, Link D and Font J A 2010 *Class. Quantum Grav.* **27** 114105
[9] Rezzolla L, Giacomazzo B, Baiotti L, Granot J, Kouveliotou C and Aloy M A 2011 *Astrophys. J. Lett.* **732** L6
[10] Howell E, Regimbau T, Corsi A, Coward D and Burman R 2011 *Mon. Not. R. Astron. Soc.* **410** 2123
[11] Lasky P D, Haskell B, Ravi V, Howell E J and Coward D M 2014 *Phys. Rev. D* **89** 047302

[12] Rosswog S, Korobkin O, Arcones A, Thielemann F K and Piran T 2014 *Mon. Not. R. Astron. Soc.* **439** 744
[13] Ravi V and Lasky P D 2014 *Mon. Not. R. Astron. Soc.* **441** 2433
[14] Gao H, Zhang B and Lü H J 2016 *Phys. Rev. D* **93** 044065
[15] Radice D, Perego A, Bernuzzi S and Zhang B 2018 *Mon. Not. R. Astron. Soc.* **481** 3670
[16] Ai S, Gao H and Zhang B 2020 *Astrophys. J.* **893** 146
[17] Xing Z Z 1994 *Phys. Rev. D* **50** R2957
[18] Ruffert M, Janka H T and Schaefer G 1996 *Astron. Astrophys.* **311** 532
[19] Shibata M and Uryū K ō 2000 *Phys. Rev. D* **61** 064001
[20] Hotokezaka K, Kiuchi K, Kyutoku K, Muranushi T, Sekiguchi Y i, Shibata M and Taniguchi K 2013 *Phys. Rev. D* **88** 044026
[21] Maione F, De Pietri R, Feo A and Löffler F 2017 *Phys. Rev. D* **96** 063011
[22] Baiotti L, Giacomazzo B and Rezzolla L 2008 *Phys. Rev. D* **78** 084033
[23] Kiuchi K, Sekiguchi Y, Shibata M and Taniguchi K 2009 *Phys. Rev. D* **80** 064037
[24] Kiuchi K, Kyutoku K, Sekiguchi Y and Shibata M 2018 *Phys. Rev. D* **97** 124039
[25] Zhang C M, Wang J, Zhao Y H, *et al.* 2010 *Astron. Astrophys.* **2011** 527
[26] Miao H, Yang H and Martynov D 2018 *Phys. Rev. D* **98** 044044
[27] Ganapathy D, McCuller L, Rollins J G, Hall E D, Barsotti L and Evans M 2021 *Phys. Rev. D* **103** 022002
[28] Wanderman D and Piran T 2015 *Mon. Not. R. Astron. Soc.* **448** 3026
[29] Sun H, Zhang B and Li Z 2015 *Astrophys. J.* **812** 33
[30] Yüksel H, Kistler M D, Beacom J F and Hopkins A M 2008 *Astrophys. J.* **683** L5
[31] Ade P A R, Aghanim N, Arnaud M, *et al.* 2016 *Astron. Astrophys.* **594** A13
[32] Abbott B P, Abbott R, Abbott T D, *et al.* 2020 *Living Rev. Relativ.* **23** 3